Table 2. Comparison of measured chemical shifts in wt and mutant MoPrP(89–143) peptides

	Expected chemical shifts		Experimental chemical shifts	
Label	α-Helix	β-Sheet	wt*	P101L, converted
G93 C_α	Unknown	43.2	42.8	42.3
A114 C_α	52.5	48.7	52.6; 48.3	48.4
V120 C_α	65.5	58.3	64.1; 57.8	58.1
A132 C_β	15.1	20.1	15.05; 20.88	20.6
M128 C_0	175.1	170.6	174.9; 170.6†	170.4
G141 C_0	171.8	168.5	170.6†; 169.3	168.9

Typical α-helical and β-sheet chemical shifts of peptides in solids are listed. All chemical shifts are in ppm, externally referenced to tetramethylsilane via the $^{13}C_0$ resonance in glycine (176.04 ppm).

*Two conformations were present in the wt peptide. Shifts for both conformations are listed, with the α-helical chemical shifts listed first.

†The M128 C_0 sheet chemical shift overlaps with the G141 C_0 helix chemical shift, and so the two cannot be distinguished in the spectra.

corresponding to residues 90–144. In this article we have chosen to use the equivalent mouse residue numbers to facilitate comparison with the mouse peptides. The SHa(89–143) peptide is relatively homogeneous in conformation when dried from water, with probes at positions A119 and A132 indicating helical conformations (Fig. 3*A*). This peptide did not aggregate or form fibrils upon treatment with acetonitrile/water and hence could not be studied in that form. A variant of the peptide carrying three alanine to valine mutations, at positions 112, 114, and 117, also was made, dramatically reducing the intrinsic helical propensity of the peptide. When dried from water, the SHa PrP(89–143, 3AV) peptide showed doubling of resonances, indicating two conformers, an extended form in addition to the helical form (Fig. 3*B*). The C_α labels at V114 and A119 indicate a predominant β-sheet conformation, with a smaller population of α-helix whereas A132 has a higher population of helical conformers than β-sheet, although β-sheet is substantially increased relative to the wt peptide. The mutant SHaPrP(89–143, 3AV) peptide has been shown to aggregate when left in cold acetonitrile/acetate-buffered saline solution, as does MoPrP(89–143,P101L), although long fibrils were not seen with electron microscopy. The spectra of the mutant SHaPrP(89–143, 3AV) peptide in the aggregated form show a further increase in the population of the extended conformers, very analogous to what was found for the MoPrP(89–143, P101L) peptide. Because of the sequence differences, some of the ^{13}C isotopic labels were different from those used for the P101L peptide. The labels used are listed in Table 1. The chemical shifts of all of the ^{13}C resonances in Fig. 3 are listed in Table 3. These results confirm the lability of the region in PrP containing residues 89–143 and show that the conformation and ability to form β-rich fibrils and aggregates are highly sensitive to point mutations. The mutations affect the global peptide conformation because sites far from the mutations show altered conformations. Although the conformational preference could be propagated through the peptide, it seems more likely that packing of peptides into aggregates is responsible for the long-range effects, and that the sequence effects reflect the ability of the peptides to form ordered quaternary structures.

Conclusions

Using solid-state ^{13}C NMR, the secondary structure in PrP(89–143) peptides was probed in different aggregated states. The wt MoPrP(89–143) peptide exists in a variety of helical and extended conformations. Although the mutant MoPrP(89–143, P101L) also exhibits some degree of conformational heterogeneity, it is clear that the mutation drives the overall conformation

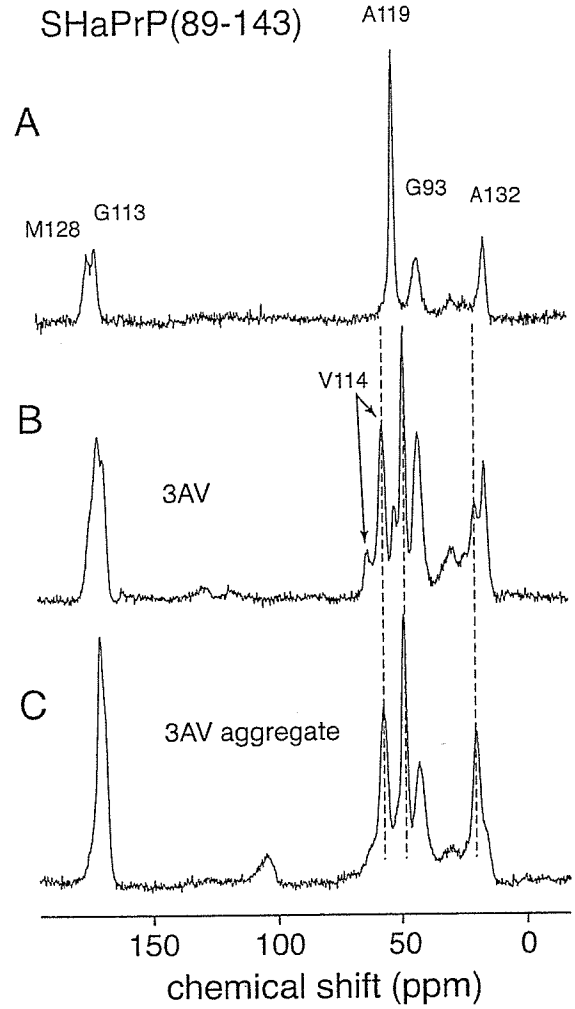

Fig. 3. Seventy-six-megahertz solid-state ^{13}C CPMAS spectra of the SHaPrP(89–143) peptide, acquired at a spinning speed of 10 kHz. (*A*) Spectrum of the wt SHaPrP(89–143) peptide dried from water. (*B*) Spectrum of the mutant SHaPrP(89–143, 3AV) peptide dried from water. (*C*) Spectrum of mutant SHaPrP(89–143, 3AV) peptide after conversion to an aggregated form by precipitation from acetonitrile/water. The lines superimposed over the resonances for V114, A119, and A132 mark the β-sheet chemical shifts.

of the peptide toward extended, β-sheet-like conformations. Furthermore, the fact that this effect occurs throughout the peptide indicates that residues 89–143 of the PrP are structurally pliable and that mutations within this region have long-range

Table 3. Comparison of measured chemical shifts in wt and mutant SHaPrP(89–143)

	Expected chemical shifts		Experimental chemical shifts	
Label	α-Helix	β-Sheet	wt	3AV, converted
G93 C_α	Unknown	43.2	42.8	42.8
G113 C_0	171.8	168.5	171.7	169.5
V114 C_α	65.5	58.3	—	57.6
A119 C_α	52.5	48.7	52.0	49.2
A132 C_α	15.1	20.1	15.6	20.6
M128 C_0	175.1	170.6	174.7	170.8

Typical α-helical and β-sheet chemical shifts in solid-state peptides are listed. All chemical shifts are in ppm, externally referenced to tetramethylsilane via the $^{13}C_0$ resonance in glycine (176.04 ppm).

effects on the conformation in ordered states, which is very likely through cooperative formation of the fibrillar aggregates. The increased linewidth in the spectra of the fibrillar form suggests that some conformational heterogeneity may still exist, at least for some sections of the peptide. Analogous results were found for the wt and mutant SHaPrP peptides. When dried from water, the sites probed in wt SHaPrP(89–143) were found to be substantially helical; however, introduction of the valine to alanine mutations profoundly changed the structure of the peptide. Probing sites throughout the mutant SHaPrP(89–143, 3AV) peptide indicated an increased population of extended conformers with these β-rich forms dominating strongly in the fibrillar state.

The *in vitro*-prepared, fibrillar form of the MoPrP(89–143, P101L) peptide stimulates disease in transgenic mice whereas other forms do not, indicating that the formation of a specific β-sheet conformation may be necessary for the peptide to become "infectious." This behavior of the mutant peptide correlates with observations on PrP in transgenic mice and humans with Gerstmann-Straussler-Scheinker disease. The mutant SHaPrP(89–143, 3AV) peptide formed aggregates rich in β-sheet like the MoPrP(89–143, P101L) peptide, whereas the wt SHaPrP(89–143) did not. The mutant SHaPrP(89–143, 3AV) peptide has not been found to cause disease in animals; however, introduction of mutations may cause an artificial "species barrier" and animals expressing a transgene with these mutations develop neurologic disease spontaneously (26). The present work makes clear that mutations strongly affect the conformational preferences of the peptides in ordered forms, and it seems likely that analogous effects occur through other disease-causing mutations. Even if the stimulation of neurodegeneration by the mutant MoPrP(89–143, P101L) peptide does not perfectly recapitulate all aspects of prion diseases, it seems to be a valuable model system for understanding features of the conformational change that PrP^{c} undergoes as it is converted into PrP^{Sc}.

D.D.L. was supported by a Howard Hughes Medical Institute predoctoral fellowship. We also acknowledge funding through National Institutes of Health Grant AG-10770, and support through the Director, Office of Energy Research, Office of Basic Energy Sciences, Materials Sciences Division of the U.S. Department of Energy under Contract No. DE-AC03-76SF00098.

1. Prusiner, S. B. (1982) *Science* **216,** 136–144.
2. Prusiner, S. B. (1998) *Proc. Natl. Acad. Sci. USA* **95,** 13363–13383.
3. Riek, R., Hornemann, S., Wider, G., Billeter, M., Glockshuber, R. & Wüthrich, K. (1996) *Nature (London)* **382,** 180–182.
4. Pan, K.-M., Baldwin, M., Nguyen, J., Gasset, M., Serban, A., Groth, D., Mehlhorn, I., Huang, Z., Fletterick, R., Cohen, F. E. & Prusiner, S. B. (1993) *Proc. Natl. Acad. Sci. USA* **90,** 10962–10966.
5. Riek, R., Hornemann, S., Wider, G., Glockshuber, R. & Wüthrich, K. (1997) *FEBS Lett.* **413,** 282–288.
6. James, T. L., Liu, H., Ulyanov, N. B., Farr-Jones, S., Zhang, H., Donne, D. G., Kaneko, K., Groth, D., Mehlhorn, I., Prusiner, S. B. & Cohen, F. E. (1997) *Proc. Natl. Acad. Sci. USA* **94,** 10086–10091.
7. Donne, D. G., Viles, J. H., Groth, D., Mehlhorn, I., James, T. L., Cohen, F. E., Prusiner, S. B., Wright, P. E. & Dyson, H. J. (1997) *Proc. Natl. Acad. Sci. USA* **94,** 13452–13457.
8. Kaneko, K., Ball, H. L., Wille, H., Zhang, H., Groth, D., Torchia, M., Trembley, P., Safar, J., Prusiner, S. B., De Armond, S. J., *et al.* (2000) *J. Mol. Biol.* **295,** 997–1007.
9. Prusiner, S. B., Groth, D., Bolton, D. C., Kent, S. B. & Hood, L. E. (1984) *Cell* **38,** 127–134.
10. Kitamoto, T., Iizuka, R. & Tateishi, J. (1993) *Biochem. Biophys. Res. Commun.* **192,** 525–531.
11. Supattapone, S., Bosque, P., Muramoto, T., Wille, H., Aagaard, C., Peretz, D., Nguyen, H. O., Heinrich, C., Torchia, M., Safar, J., *et al.* (1999) *Cell* **96,** 869–878.
12. Muramoto, T., Scott, M., Cohen, F. E. & Prusiner, S. B. (1996) *Proc. Natl. Acad. Sci. USA* **93,** 15457–15462.
13. Gasset, M., Baldwin, M., Lloyd, D. H., Gabriel, J.-M., Holtzman, D. M., Cohen, F. E., Fletterick, R. & Prusiner, S. B. (1992) *Proc. Natl. Acad. Sci. USA* **89,** 10940–10944.
14. Come, J. H., Fraser, P. E. & Lansbury, P. T. (1993) *Proc. Natl. Acad. Sci. USA* **90,** 5959–5963.
15. Forloni, G., Angeretti, N., Chiesa, R., Monzani, E., Salmoni, M., Bugiani, O. & Tagliavini, F. (1993) *Nature (London)* **362,** 543–546.
16. Tagliavini, F., Prelli, F., Verga, L., Giaccone, G., Sarma, R., Gorevic, P., Ghetti, B., Passerinin, F., Ghibaudi, E., Forloni, G., *et al.* (1993) *Proc. Natl. Acad. Sci. USA* **90,** 9678–9682.
17. Zhang, H., Kaneko, K., Nguyen, J., Livshits, T. L., Baldwin, M., Cohen, F. E., James, T. L. & Prusiner, S. B. (1995) *J. Mol. Biol.* **250,** 514–526.
18. Nguyen, J., Baldwin, M., Cohen, F. E. & Prusiner, S. B. (1995) *Biochemistry* **34,** 4186–4192.
19. Heller, J., Kolbert, A. C., Larsen, R., Ernst, M., Bekker, T., Baldwin, M., Prusiner, S. B., Pines, A. & Wemmer, D. E. (1996) *Protein Sci.* **5,** 1655–1661.
20. Kaneko, K., Wille, H., Mehlhorn, I., Zhang, H., Ball, H. L., Cohen, F. E., Baldwin, M. & Prusiner, S. B. (1997) *J. Mol. Biol.* **270,** 574–586.
21. Saito, H., Tabeta, R., Shojoi, A. & Ozaki, T. (1983) *Macromolecules* **16,** 1050–1057.
22. Saito, H. (1986) *Magn. Reson. Chem.* **24,** 835–852.
23. Spera, S. & Bax, A. (1991) *J. Am. Chem. Soc.* **113,** 5490–5492.
24. Wishart, D. S. & Sykes, B. D. (1994) *J. Biomol. NMR* **4,** 171–180.
25. Bennett, A. E., Rienstra, C. M., Auger, M., Lakshmi, K. V. & Griffin, R. G. (1995) *J. Chem. Phys.* **103,** 6951–6958.
26. Hegde, R. S., Tremblay, P., Groth, D., DeArmond, S. J., Prusiner, S. B. & Lingappa, V. R. (1999) *Nature (London)* **402,** 822–826.

Antibodies inhibit prion propagation and clear cell cultures of prion infectivity

David Peretz*, R. Anthony Williamson†, Kiotoshi Kaneko*‡, Julie Vergara*, Estelle Leclerc†, Gerold Schmitt-Ulms*, Ingrid R. Mehlhorn*, Giuseppe Legname*, Mark R. Wormald§, Pauline M. Rudd§, Raymond A. Dwek§, Dennis R. Burton†‖ & Stanley B. Prusiner*¶#

** Institute for Neurodegenerative Diseases and Departments of ¶ Neurology and # Biochemistry and Biophysics, University of California, San Francisco, California 94143-0518, USA*
† Departments of Immunology and ‖ Molecular Biology, The Scripps Research Institute, La Jolla, California 92037, USA
§ The Glycobiology Institute, Department of Biochemistry, University of Oxford, Oxford OX1 3QU, UK

Prions are the transmissible pathogenic agents responsible for diseases such as scrapie and bovine spongiform encephalopathy. In the favoured model of prion replication, direct interaction between the pathogenic prion protein (PrP^{Sc}) template and endogenous cellular prion protein (PrP^{C}) is proposed to drive the formation of nascent infectious prions[1,2]. Reagents specifically binding either prion-protein conformer may interrupt prion production by inhibiting this interaction. We examined the ability of several recombinant antibody antigen-binding fragments (Fabs) to inhibit prion propagation in cultured mouse neuroblastoma cells (ScN2a) infected with PrP^{Sc}. Here we show that antibodies binding cell-surface PrP^{C} inhibit PrP^{Sc} formation in a dose-dependent manner. In cells treated with the most potent antibody, Fab D18, prion replication is abolished and pre-existing PrP^{Sc} is rapidly cleared, suggesting that this antibody may cure established infection. The potent activity of Fab D18 is associated with its ability to better recognize the total population of PrP^{C} molecules on the cell surface, and with the location of its epitope on PrP^{C}. Our observations support the use of antibodies in the prevention and treatment of prion diseases and identify a region of PrP^{C} for drug targeting.

To study inhibition of prion propagation by antibodies, we used recombinant prion protein-specific Fabs D13, D18, R1, R2, E123, E149 and R72 (refs 3–6). The binding epitopes and affinity constants of the antibodies for recombinant prion protein are shown in Supplementary Information Table 1. Fab R72 does not recognize prion protein in surface plasmon resonance (SPR) or on the cell surface, but does bind to PrP^{C} coated onto the surface of wells for enzyme-linked immunosorbent assay (ELISA)[4].

A range of concentrations of each antibody was added to ScN2a cultures for 7 days. Cells were then collected and the level of PrP^{Sc} in the culture analysed by immunoblotting. The level of PrP^{Sc} in cells

‡ Present address: National Institute of Neuroscience, Tokyo 187-8502, Japan.

treated with Fabs D13, D18, R1 and R2, compared with that in non-treated cells, was dramatically reduced in a dose-dependent manner (Fig. 1). By this analysis, Fabs D13 and D18 seem to be about equally effective: their values for 50%-inhibitory concentration (IC_{50}) were 0.6 μg ml^{-1} (12 nM) and 0.45 μg ml^{-1} (9 nM), respectively. Fabs R1 and R2 were slightly less efficient, with IC_{50} values of 2.5 μg ml^{-1} (50 nM) and 2.0 μg ml^{-1} (40 nM), respectively. In contrast, 7-day treatment with Fabs E123, E149 or R72, or 5-day treatment with polyclonal immunglobulin-γ (IgG) recognizing both transmembrane and glycosyl phosphatidylinositol (GPI)-anchored forms of mouse neural cell-adhesion molecules (N-CAM)[7], did not reduce the level of PrP^{Sc} in ScN2a cultures even when these antibodies were used at high concentrations (Fig. 1). During these experiments, the levels of PrP^{C} and glyceraldehyde-3-phosphate dehydrogenase in antibody-treated and untreated cells were found to be invariant (see Supplementary Information Fig. 1), indicating that the prion protein-specific antibodies used produced no cytotoxic effects that may have indirectly compromised the production of PrP^{Sc}.

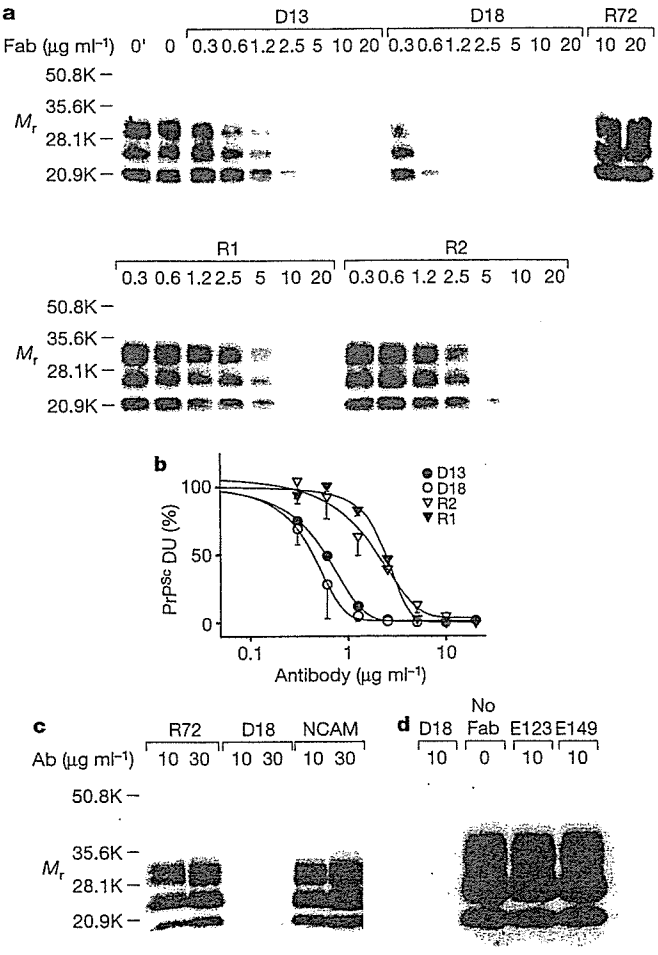

Figure 1 Dose-dependent inhibition of PrP^{Sc} formation in cells by prion protein-specific recombinant antibody Fabs. **a**, PrP^{Sc} levels in ScN2a cells were measured by immunoblotting after 7 d of culture in the presence of antibodies D13, D18, R72, R1 or R2 at 0–20 μg ml^{-1}. Lane 0′ indicates the level of PrP^{Sc} in the ScN2a culture before antibody treatment. Protein size is shown as relative molecular mass (M_r), in thousands (K). **b**, Densitometric measurement of PrP^{Sc} bands identified in the immunoblot in **a**. Values are given as densitometric units (DU), where 100% is equivalent to the intensity of the PrP^{Sc} band in the absence of antibody treatment and 0% denotes undetectable levels of PrP^{Sc} in the culture (no band). Data represent the mean from three independent experiments. **c**, **d**, PrP^{Sc} levels in ScN2a cells cultured for 5 d in the presence of anti-N-CAM polyclonal IgG (**c**), or for 7 d in the presence of Fabs E123 and E149 (**d**).

We then determined whether PrP^{Sc} remained undetectable after removal of prion protein-specific antibody. ScN2a cells were independently passaged (serially subcultured) for at least 7 days in the presence of 10 μg ml^{-1} of each of the recombinant Fabs. Antibody was then removed from the culture and the cells passaged for an additional period in Fab-free medium, after which time the level of PrP^{Sc} was re-measured (Fig. 2). PrP^{Sc} concentrations in ScN2a cells passaged for 1 week in the presence of Fab D18 were reduced to non-detectable levels, but returned to about 50% of the level of an untreated control culture after 1 additional week of growth in the absence of D18. However, if cells were cultured for a 2-week period in the presence of Fab D18 then PrP^{Sc} remained at undetectable levels after 4 additional weeks of culture in antibody-free medium. Similarly, when prion-infected cells were treated with Fab D13 for 3 consecutive weeks followed by 1 week of growth in media without antibody, no PrP^{Sc} could be detected, although after an additional week in culture without Fab, PrP^{Sc} increased back to 5% of the level found in untreated control culture. If, however, cells were subjected to 4 consecutive weeks of treatment with Fab D13, PrP^{Sc} remained below the level of detection after 4 weeks of culture without antibody (data not shown). When used at a concentration of 10 μg ml^{-1} neither Fab R1 nor Fab R2 was sufficiently potent to prevent the re-emergence of PrP^{Sc} in the culture after antibody was removed. Fab R72 had no impact on the level of PrP^{Sc} in the culture after 3 or 9 (data not shown) consecutive weeks of treatment.

As a second measure of prion titre, we performed bioassays in which CD-1 Swiss mice were inoculated with antibody-treated (10 μg ml^{-1}) and untreated ScN2a cells. Mice inoculated intracerebrally with Fab D18-, D13- or even R2-treated cells were free of disease after 265 days, whereas mice inoculated with untreated or R72-treated cells had a mean incubation time to disease of 169 and 165 days, respectively. The prolonged incubation times correspond to a reduction of over three orders of magnitude in the infectious prion titre in treated cells[8].

The above data might be taken to indicate that PrP^{Sc} levels rapidly diminish in the presence of specific antibody. Indeed, other studies describing the inhibition of prion propagation[9–13] have been interpreted in this way. However, if an antibody or other reagent curtails the formation of nascent PrP^{Sc} molecules, each round of cell division may serve to dilute the effective concentration, but not necessarily the total amount, of PrP^{Sc} within the culture.

To more thoroughly analyse the kinetics of prion clearance,

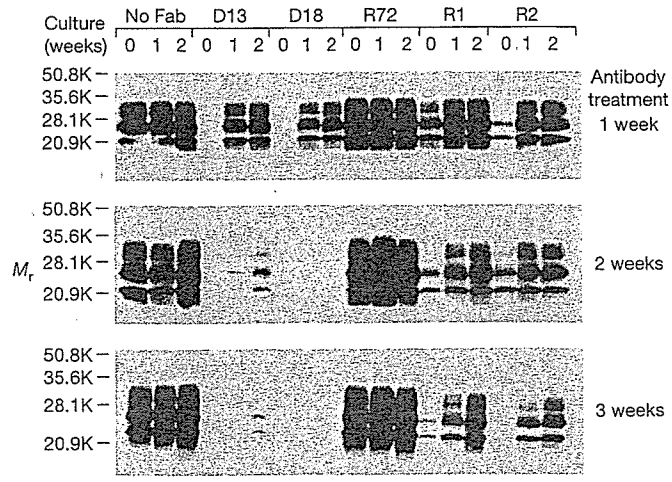

Figure 2 Elimination of PrP^{Sc} from prion-infected cells treated with antibodies. ScN2a cells were cultured for 1, 2 or 3 weeks in 10 μg ml^{-1} of either Fab D13, D18, R72, R1 or R2, or in the absence of antibody. The level of PrP^{Sc} in the culture was then analysed by immunoblot either immediately after the termination of antibody treatment (lane 0) or after cells were passaged for an additional 1 (lane 1) or 2 (lane 2) weeks in the absence of antibody.

ScN2a cells were independently grown in the presence of 10 μg ml^{-1} of prion protein-specific Fabs. Cells were collected after 1, 2, 3 or 4 days of antibody treatment, and the total mass of cell protein was determined in each case as a measure of cell number. The PrP^{Sc} concentrations were determined by immunoblotting and the total PrP^{Sc} in the culture at each point was calculated by factoring in the total cell mass in each case (Fig. 3).

In agreement with earlier results, Fab D18 was found to be the most effective antibody. The time taken from the initial treatment with Fab D18 to eliminate 50% of PrP^{Sc} from the cells (half-life) was 28 h. The half-life of PrP^{Sc} in ScN2a cells is thought to exceed 24 h (ref. 14), suggesting that, at a concentration of 10 μg ml^{-1}, Fab D18 is able to completely abolish prion propagation and that pre-existing PrP^{Sc} is subsequently eliminated from the cells. This finding indicates that a certain amount of PrP^{Sc} is continuously expunged from ScN2a cultures through normal degradation pathways. Fab D13 was the next most potent antibody, also lowering the level of PrP^{Sc} in the culture, but to a lesser extent than Fab D18, indicating that there may be a minimal level of residual PrP^{Sc} synthesis in the presence of this Fab. Fabs R1 and R2, although reducing the rate of prion propagation in ScN2a cells, are not sufficiently effective to yield a reduction in the quantity of PrP^{Sc} in the culture. In untreated cultures, or cultures treated with Fab R72, prion propagation remained unaffected, and PrP^{Sc} levels increased in tandem with growth in the ScN2a cell population.

The inhibitory effect we observe is most readily explained by antibodies binding specifically to PrP^{C} molecules on the cell surface and thereby hindering the docking of PrP^{Sc} template or a cofactor critical for the conversion of PrP^{C} to PrP^{Sc}. In agreement with this hypothesis, Fab D18, which was by far the most effective antibody we evaluated, was distinguished by its capacity to bind a significantly greater number of cell-surface PrP^{C} molecules than any of the other antibodies tested (see Supplementary Information Fig. 2).

To address whether the region of prion protein bound by each antibody was of intrinsic importance to its inhibitory potency, we compared inhibition at conditions in which equal amounts of two different Fabs were bound to the ScN2a cell surface. When used at concentrations of 0.6 μg ml^{-1}, equivalent amounts of Fabs D18 and D13 were bound to the cell surface but D18 inhibited prion replication much more efficiently (Fig. 1a). Similarly, at concentrations of 0.6 μg ml^{-1} and 2.5 μg ml^{-1}, respectively, Fabs D18 and R1 bound equivalently to ScN2a cells, but D18 was clearly more effective in reducing the level of PrP^{Sc} in the culture. Finally, at a concentration of 2.5 μg ml^{-1}, Fabs D13 and R1 bound equivalently to the cell surface, but D13 more actively reduced PrP^{Sc} synthesis.

The demonstration that the region of PrP^{C} bound by a given antibody is a critical determinant of its inhibitory capacity provides insight into the specific machinery of prion propagation. The known binding epitope of Fab D18 spans prion protein residues 132–156 (ref. 5) and incorporates helix A (residues 145–155) of PrP^{C} (Fig. 4). Spatially, this sequence is positioned on the opposite face of the protein from residues Q167, Q171, T214 and Q218, which are thought to participate in binding an auxiliary molecule essential to prion propagation[15,16]. We therefore argue that D18 operates mechanistically by directly blocking or modifying PrP^{C} interaction with PrP^{Sc}, rather than by inhibiting the binding of a cofactor. A number of other reports also identify the 132–156 region of the protein as critical to prion synthesis and between-species transmission[17–20], although prion propagation can proceed in the absence of sequence between residues 140 and 175 (ref. 21), indicating that helix A of PrP^{C} is not a prerequisite for PrP^{Sc} binding. Together, these studies identify the 132–140 portion of PrP^{C} as a logical target for development of anti-prion drugs.

Significantly, with the exception of Fabs R1 and R2, none of the antibodies we have used in this study competes efficiently with the others for binding to cell-surface PrP^{C} (E.L., unpublished data). This suggests that, in therapeutic strategies, the antibodies may be used in combination to achieve maximum inhibitory effect.

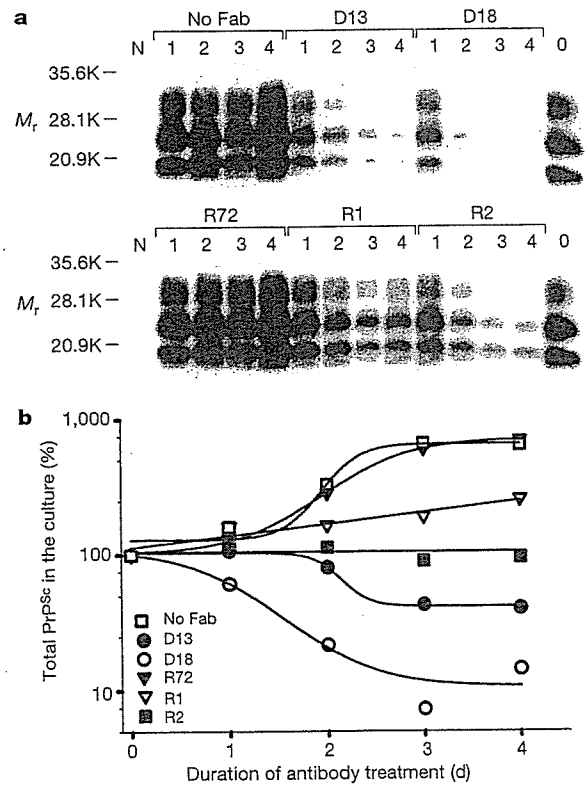

Figure 3 Time course of antibody-mediated PrP^{Sc} clearance. **a**, The level of PrP^{Sc} in ScN2a cells grown for 1, 2, 3 or 4 d in the presence of prion protein-specific Fabs (10 μg ml^{-1}) was determined by immunoblotting. **b**, The effect of antibody treatment on the total amount of PrP^{Sc} in ScN2a cell cultures. Lane N indicates N2a cells treated with proteinase K. The data represent the mean of three experiments.

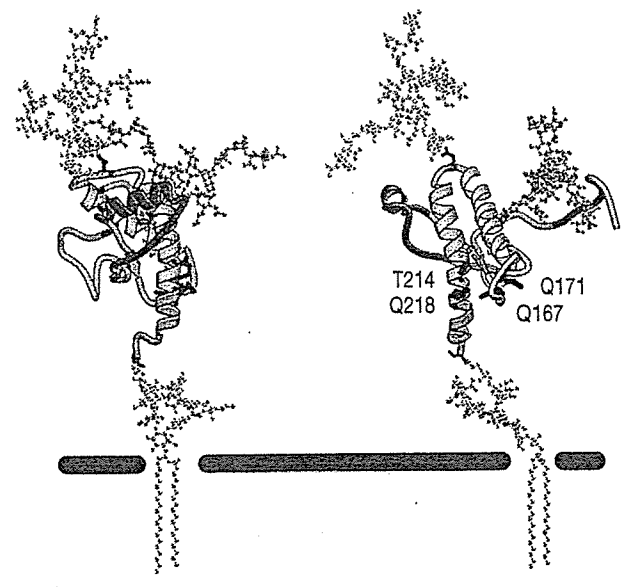

Figure 4 Regions of sequence recognized by Fabs D13 (blue), D18 (red), and R1 and R2 (green) superimposed onto two views of the structure of recombinant prion protein (90–231) determined by nuclear magnetic resonance[27]. Carbohydrate moieties linked to Asn 180 and Asn 196 are shown in orange and yellow, respectively[28,29]. The COOH-terminal GPI anchor is shown in cyan extending into the cell membrane (black). Side chains of residues Q167, Q171, T214 and Q218, which are proposed to bind to a cellular cofactor critical to prion propagation, are included (purple).

We have shown that antibodies binding to defined regions of PrP^C effectively inhibit prion replication. For *in vivo* applications, Fab fragments have the disadvantage of a short half-life, and may not efficiently traverse from the peripheral circulation into the central nervous system. Whole-antibody molecules prepared from the Fabs will probably be more useful, but may require engineering to prevent the recruitment of immunological effector mechanisms to antibody-coated cells[22,23]. Our studies, in combination with advances targeting Alzheimer disease[24,25], indicate that specific antibodies may become a powerful weapon in the fight against neurodegenerative diseases associated with the accumulation of misfolded proteins. □

Methods

Expression and purification of antibodies

Escherichia coli strain 33B6 was transformed with plasmids encoding prion protein-specific Fabs, and fermented for 48 h using a Biostat B controller (Braun) and 11 media containing MT-8 salts (0.26 g l^{-1} K_2HPO_4, 0.13 g l^{-1} $NaH_2PO_4.2H_2O$, 0.5 g l^{-1} NH_4SO_4, 0.1 g l^{-1} $C_6H_5Na_3O_7.2H_2O$ and 0.15 g l^{-1} KCl), 0.5 g isoleucine, 20% NZ amines, 20% yeast extract, 1 mM $MgSO_4$, 50% glucose, trace metals and 100 μg ml^{-1} ampicillin. Bacterial paste was resuspended in 5 volumes of 2 mM imidazole, 20 mM Na_2HPO_4, and 250 mM NaCl, pH 7.0, and processed twice in a Microfluidizer M-110 EH (Microfluidics). The processed paste was titrated to 0.1% polyethylenimine (5% stock solution, pH 8.0) and stirred at 4 °C for 30 min, then centrifuged at 12,000*g* for 30 min at 4 °C. The supernatant was diluted in an equal volume of 20 mM imidazole, pH 7.0, and loaded onto an SP Fast Flow Sepharose column (Amersham). Recombinant Fab was eluted with a linear gradient of 0–100% of 20 mM imidazole, 500 mM sodium acetate, pH 7.0, then directly applied to a column for immobilizing by metal-affinity chromatography (IMAC). Antibody was eluted from this column with 200 mM imidazole, pH 7.0, then thoroughly dialysed at 4 °C against 10 mM Tris-HCl buffer, pH 7.2. The dialysed samples were further purified by elution from a QS Fast Flow Sepharose column using a linear gradient of 0–100% of 10 mM Tris-HCl buffer, pH 7.2, and 500 mM NaCl, and sterilized by filtration.

Cell culture

Mouse neuroblastoma cells (N2a) were obtained from the American Type Culture Collection. Prion-infected mouse neuroblastoma (ScN2a) cells have been described previously[8,26]. Stock cultures of ScN2a and N2a cells were maintained in MEM, 10% fetal bovine serum (FBS), 2 mM Glutamax (GIBCO BRL), 100 units ml^{-1} penicillin and 100 μg ml^{-1} streptomycin sulphate in a humidified 37 °C incubator with 5% CO_2. Cells were split 1:15 weekly using 0.05% (w/v) trypsin-EDTA (GIBCO BRL).

Studies of antibody inhibition

Antibodies were added to 2×10^5 ScN2a cells and incubated for an appropriate time according to individual experimental protocols. The cells were fed three times per week with replacement media containing the appropriate amount of antibody. In inhibition experiments in which ScN2a cultures required splitting, cells were detached from culture plates using cell dissociation buffer (GIBCO BRL), rather than with trypsin, because enzymatic activity may have modulated the level of PrP^{Sc}. Cells were collected *in situ* by washing three times with calcium- and magnesium-free PBS and resuspending in 1 ml lysis buffer (10 mM Tris, pH 7.5, containing 150 mM NaCl, 0.5% sodium deoxycholate, 0.5% nonident P-40). Cell nuclei were removed from the lysate by centrifugation at 2,000*g* for 2 min, and the protein concentration of the supernatant measured by bicinchoninic acid assay (BCA, Pierce).

Quantification of PrP^{Sc}

ScN2a cell lysates (1 mg ml^{-1}) were treated with 20 μg ml^{-1} of proteinase K (total protein : enzyme ratio, 50:1) for 1 h at 37 °C. Proteolytic digestion was terminated by the addition of phenylmethyl sulphonyl fluoride (PMSF) to a final concentration of 2 mM. Forty micrograms of the digested cell lysate was mixed with an equal volume of 2 × non-reducing SDS sample buffer, boiled for 5 min, cleared by centrifugation and resolved by SDS–PAGE (14%). Samples were electroblotted onto membranes of polyvinylidene fluoride (PVDF) and blocked with 5% (w/v) non-fat milk protein in calcium- and magnesium-free PBS. Prion protein was detected using 0.5 μg ml^{-1} D18 antibody cross-linked to pre-activated amine-reactive horseradish peroxidase (Pierce). Blots were developed with enhanced chemiluminescence (ECL) reagent (Amersham) for 1 min, and exposed to ECL Hypermax film (Amersham). Densitometric scanning of PrP^{Sc} bands was performed with a Chemi Imager 4000 Low Light Imaging System using AlphaEase software version 3.3e (Alpha Innotech). Apparent amounts of PrP^{Sc} (densitometric units) were plotted as a percentage of PrP^{Sc} found in equivalent untreated ScN2a cell cultures on the day of collection. Levels of PrP^C were determined similarly, except that N2a lysates were not digested with proteinase K.

Bioassays

Antibody-treated (60 d) and untreated ScN2a cells were resuspended in 1 ml of PBS. Thirty microlitres of the cell resuspension were inoculated intracerebrally into groups of 10 CD-1 Swiss mice. Mice were scored daily for early and late onset of clinical signs of scrapie. Infectious titres of mouse prions in CD-1 Swiss mice were derived by use of the equation

$$\log(T) = 1.52 + \log(D) + (185 - Y)/12.66$$

where T is the ID_{50} (in units ml^{-1}), D is the dilution (defined as the fractional dilution of the diluted sample), and Y is the mean interval from inoculation to onset of terminal illness in days[8].

Flow cytometry

ScN2a cells were resuspended with cell-dissociation buffer (GIBCO BRL) and washed twice with FACS buffer (MEM, 5% (v/v) cell-dissociation buffer and 2% (v/v) FBS). Increasing concentrations of prion protein-specific Fabs were added to aliquots of 10^6 cells. After incubation for 15 min at room temperature, cells were washed four times with FACS buffer and stained for 15 min at room temperature with a 1:200 dilution in FACS buffer of fluorescein isothiocyanate (FITC)-conjugated goat anti-human IgG Fab (Jackson Immunologicals). Cells were then washed three times in FACS buffer, fixed with freshly prepared 0.4% (v/v) paraformaldehyde and analysed using the Becton Dickenson FACscan instrument.

Nomenclature

Numbering of residues corresponds to mouse prion protein throughout.

Received 19 March; accepted 23 July 2001.

1. Telling, G. C. *et al.* Evidence for the conformation of the pathologic isoform of the prion protein enciphering and propagating prion diversity. *Science* 274, 2079–2082 (1996).
2. Prusiner, S. B. Prions. *Proc. Natl Acad. Sci. USA* 95, 13363–13383 (1998).
3. Williamson, R. A. *et al.* Circumventing tolerance in order to generate autologous monoclonal antibodies to the prion protein. *Proc. Natl Acad. Sci. USA* 93, 7279–7282 (1996).
4. Peretz, D. *et al.* A conformational transition at the N-terminus of the prion protein features in formation of the scrapie isoform. *J. Mol. Biol.* 273, 614–622 (1997).
5. Williamson, R. A. *et al.* Mapping the prion protein using recombinant antibodies. *J. Virol.* 72, 9413–9418 (1998).
6. Leclerc, E. *et al.* Immobilized prion protein undergoes spontaneous rearrangement to a conformation having features in common with the infectious form. *EMBO J.* 20, 1574–1554 (2001).
7. Chuong, C.-M., McClain, D. A., Streit, P. & Edelman, G. M. Neural cell adhesion molecules in rodent brains isolated by monoclonal antibodies with cross-species reactivity. *Proc. Natl Acad. Sci. USA* 79, 4234–4238 (1982).
8. Butler, D. A. *et al.* Scrapie-infected murine neuroblastoma cells produce protease-resistant prion proteins. *J. Virol.* 62, 1558–1564 (1988).
9. Caughey, B. & Raymond, G. J. Sulfated polyanion inhibition of scrapie-associated PrP accumulation in cultured cells. *J. Virol.* 67, 643–650 (1993).
10. Chabry, J. *et al.* Species-independent inhibition of abnormal prion protein (PrP) formation by a peptide containing a conserved PrP sequence. *J. Virol.* 73, 6245–6250 (1999).
11. Perrier, V. *et al.* Mimicking dominant negative inhibition of prion replication through structure-based drug design. *Proc. Natl Acad. Sci. USA* 97, 6073–6078 (2000).
12. Caughey, W. S., Raymond, L. D., Horiuchi, M. & Caughey, B. Inhibition of protease-resistant prion protein formation by porphyrins and phthalocyanines. *Proc. Natl Acad. Sci. USA* 95, 12117–12122 (1998).
13. Supattapone, S., Nguyen, H. O., Cohen, F. E., Prusiner, S. B. & Scott, M. R. Elimination of prions by branched polyamines and implications for therapeutics. *Proc. Natl Acad. Sci. USA* 96, 14529–14534 (1999).
14. Borchelt, D. R., Scott, M., Taraboulos, A., Stahl, N. & Prusiner, S. B. Scrapie and cellular prion proteins differ in their kinetics of synthesis and topology in cultured cells. *J. Cell Biol.* 110, 743–752 (1990).
15. Kaneko, K. *et al.* Evidence for protein X binding to a discontinuous epitope on the cellular prion protein during scrapie prion propagation. *Proc. Natl Acad. Sci. USA* 94, 10069–10074 (1998).
16. Zulianello, L. *et al.* Dominant-negative inhibition of prion formation diminished by deletion mutagenesis of the prion protein. *J. Virol.* 74, 4351–4360 (2000).
17. Scott, M. *et al.* Propagation of prions with artificial properties in transgenic mice expressing chimeric PrP genes. *Cell* 73, 979–988 (1993).
18. Priola, S. A. & Chesebro, B. A single hamster PrP amino acid blocks conversion to protease-resistant PrP in scrapie-infected mouse neuroblastoma cells. *J. Virol.* 69, 7754–7758 (1995).
19. Kocisko, D. A. *et al.* Species specificity in the cell-free conversion of prion protein to protease-resistant forms: A model for the scrapie species barrier. *Proc. Natl Acad. Sci. USA* 92, 3923–3927 (1995).
20. Priola, S. A., Chabry, J. & Chan, K. Efficient conversion of normal prion protein (PrP) by abnormal hamster PrP is determined by homology at amino acid residue 155. *J. Virol.* 75, 4673–4680 (2001).
21. Supattapone, S. *et al.* Prion protein of 106 residues creates an artificial transmission barrier for prion replication in transgenic mice. *Cell* 96, 869–878 (1999).
22. Xu, D. *et al.* In vitro characterization of five humanized OKT3 effector function variant antibodies. *Cell. Immunol.* 200, 16–26 (2000).
23. Idusogie, E. E. *et al.* Mapping of the C1q binding site on rituxan, a chimeric antibody with a human IgG1 Fc. *J. Immunol.* 164, 4178–4184 (2000).
24. Schenk, D. *et al.* Immunization with amyloid-β attenuates Alzheimer-disease-like pathology in the PDAPP mouse. *Nature* 400, 173–177 (1999).
25. Bard, F. *et al.* Peripherally administered antibodies against amyloid β-peptide enter the central nervous system and reduce pathology in a mouse model of Alzheimer disease. *Nature Med.* 6, 916–919 (2000).
26. Race, R. E., Fadness, L. H. & Chesebro, B. Characterization of scrapie infection in mouse neuroblastoma cells. *J. Gen. Virol.* 68, 1391–1399 (1987).
27. James, T. L. *et al.* Solution structure of a 142-residue recombinant prion protein corresponding to the infectious fragment of the scrapie isoform. *Proc. Natl Acad. Sci. USA* 94, 10086–10091 (1997).
28. Rudd, P. M., Wormald, M. R., Wing, D. R., Prusiner, S. B. & Dwek, R. A. Prion glycoprotein: Structure, dynamics, and roles for the sugars. *Biochemistry* 40, 3759–3766 (2001).

29. Petrescu, A. J., Petrescu, S. M., Dwek, R. A. & Wormald, M. R. A statistical analysis of N- and O-glycan linkage conformations from crystallographic data. *Glycobiology* 9, 343–352 (1999).

Supplementary information is available on *Nature*'s World-Wide Web site (http://www.nature.com) or as paper copy from the London editorial office of *Nature*.

Acknowledgements

We thank J. Safar, S. DeArmond, F. Cohen and P. Dazin for discussions and K. Crossin for anti-N-CAM antibody. This work was supported by grants from the National Institutes of Health to R.A.W., D.R.B. and S.B.P.

Correspondence and requests for materials should be addressed to R.A.W. (e-mail: anthony@scripps.edu) or D.R.B. (e-mail: burton@scripps.edu).

Adv Biochem Engin/Biotechnol (2005) 95: 1–15
DOI 10.1007/b102208

Engineering Fluorescent Proteins

Atsushi Miyawaki (✉) · Takeharu Nagai · Hideaki Mizuno

Laboratory for Cell Function Dynamics, Advanced Technology Development Group, Brain Science Institute, RIKEN, 2-1 Hirosawa, Wako-city, Saitama, 351-0198 Japan
matsushi@brain.riken.jp

Abstract Green fluorescent protein from the jellyfish *Aequorea victora* (GFP) and GFP-like proteins from Anthozoa species encode light-absorbing chromophores intrinsically within their respective protein sequences. Recent studies have made progress in obtaining bright variants of these proteins which develop chromophores quickly and efficiently, as well as novel fluorescent proteins that photoactivate or photoconvert, i.e., become fluorescent or change colors upon illumination at specific wavelengths. Also, monomeric versions of these proteins have been engineered for fusion protein applications. Simple GFP variants and circularly permuted GFP variants have been used to develop fluorescent probes that sense physiological signals such as membrane potential and concentrations of free calcium. Further molecular characterization of the structure and maturation of these proteins is in progress, aimed at providing information for rational design of variants with desired fluorescence properties.

Keywords Green fluorescent protein · GFP-like proteins · Chromophore · Photoactivation · Photoconversion · Calcium imaging

List of Abbreviations

FP	Fluorescent protein
GFP	Green fluorescent protein
PA-GFP	Photoactivatable GFP
RFP	Red fluorescent protein
YFP	Yellow fluorescent protein

1 Engineering for Brighter Fluorescence

1.1 Fluorescence Development

Green fluorescent protein (GFP), originally isolated from the jellyfish *Aequorea victoria* (*Aequorea* GFP), has been the subject of continued interest since it was cloned in 1992 [1, 2]. Moreover, the discovery of novel GFP-like proteins from Anthozoans (coral animals) has significantly expanded the range of colors available for cell biological applications [3, 4]. Here, the term 'fluorescent protein' (FP) will be used to describe a protein that can become spontaneously fluorescent. Due to their autocatalytic chromophore generation, and the possibility of spectral manipulation of these proteins via mutagenesis, FPs of this sort make attractive tools for a myriad of biological applications. After protein synthesis, many FPs mature slowly through a multi-step process that consists of folding, chromophore formation, and chromophore modification. *Aequorea* GFP, for example, requires folding and chromophore formation processes, which for this protein may be interdependent [5]. Sometime during or after the protein adopts its native conformation, an internal tripeptide, Ser^{65}-Tyr^{66}-Gly^{67}, forms a chromophore, 4-(*p*-hydroxybenzylidene)-5-imidazolinone, by nucleophilic attack of Gly^{67}-Nα on the carbonyl group of Ser^{65}, followed by dehydration and oxidation of the α-β bond of Tyr^{66} (Fig. 1A). The wavelengths of light absorbed and emitted by the chromophore depend on the local chemistry, and as a result substitutions in or near the chromophore may produce large changes in fluorescence. Yellow fluorescent protein (YFP), a yellow variant of GFP, has a Tyr residue substituted at position Thr^{203} (T203Y). The π-π interaction between Tyr^{203} and the chromophore phenol ring most likely reduces the excited state energy, thereby increasing the excitation and emission wavelengths (Fig. 1B) [2]. In addition to folding and chromophore formation, some GFP-like proteins undergo a process of chromophore modification in order to reach a mature state with the desired fluorescence properties. This event takes place in the final folded molecule. For example, DsRed is a GFP-like protein that fluoresces first green and then red, implying that its chromophore structure is modified during maturation. Recent structural studies have shown that a tripeptide in DsRed (Gln^{66}-Tyr^{67}-Gly^{68}) analogous to the chromophore-forming sequence of *Aequorea* GFP forms a 4-(*p*-hydroxybenzylidene)-5-imidazolinone chro-

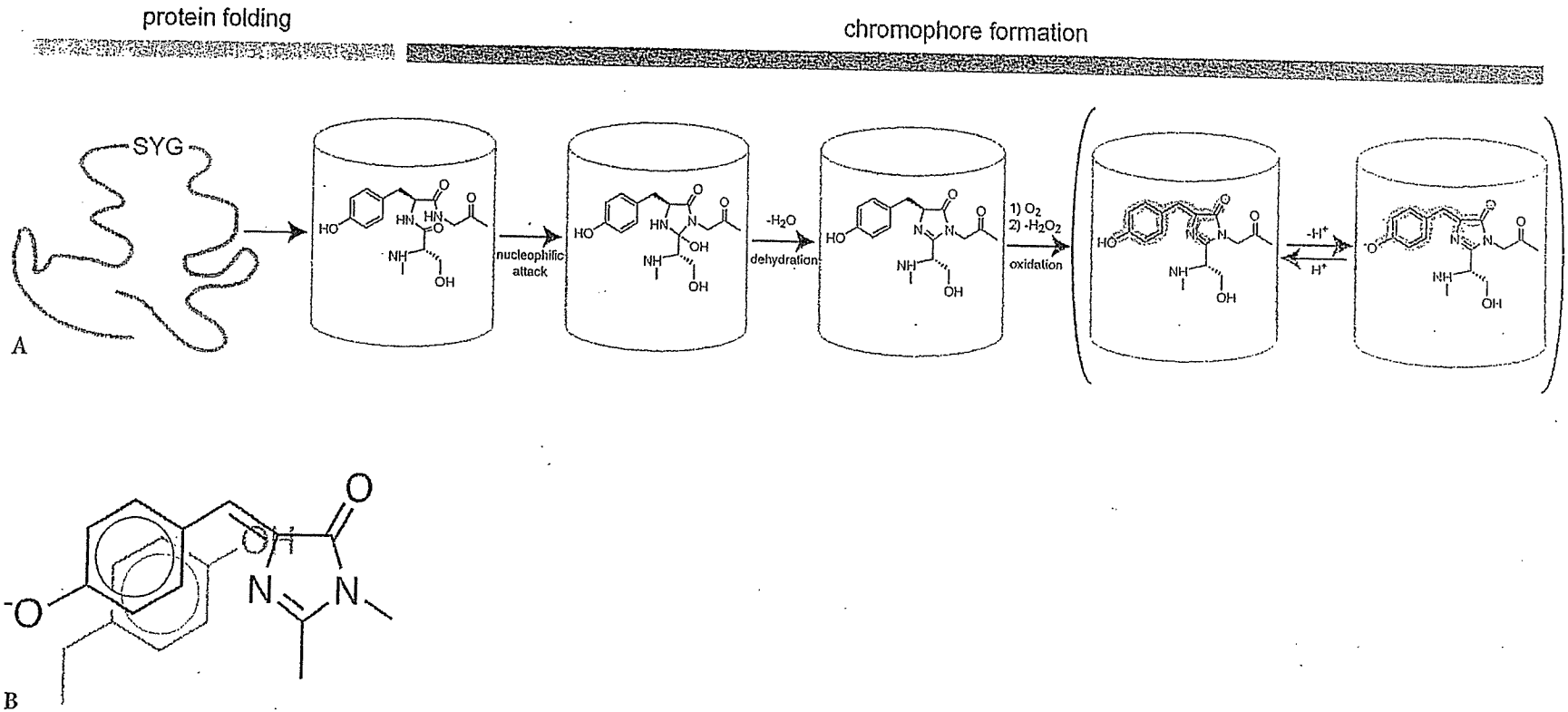

Fig. 1 A Diagram representing *Aequorea* GFP folding and chromophore formation. The β-can structure represents the native conformation of the protein, while the denatured form is depicted as an irregular chain. π-conjugation for visible-light absorption is indicated in *gray*. B Chromophore structure of YFP. Reprinted with permission from Miyawaki et al., Curr. Opin. Chem. Biol. 7, 558 (2003). Copyright © 2003 Elsevier

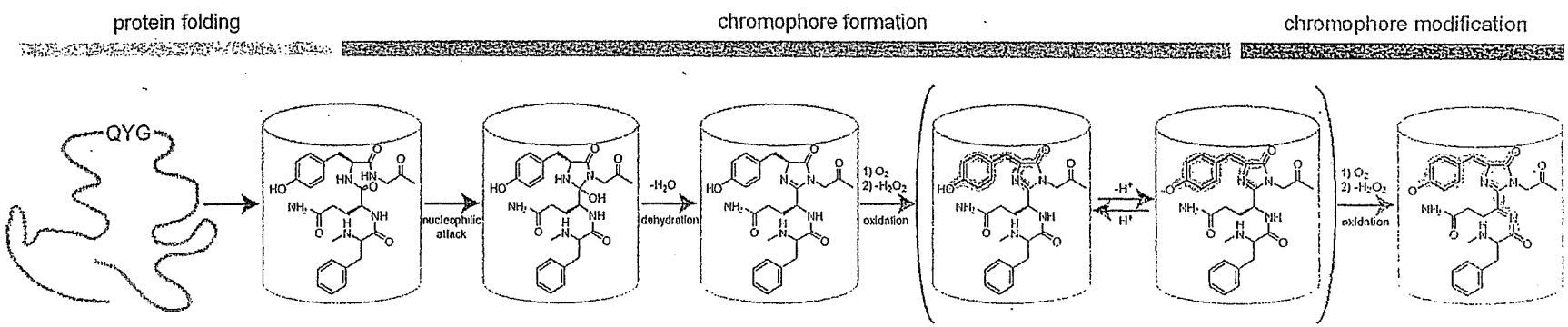

Fig. 2 Schematic of folding, chromophore formation, and chromophore modification of DsRed. The β-can structure represents the native conformation of the protein, while the denatured form is shown as an irregular chain. It is not known at which step oligomerization occurs. π-conjugation for visible-light absorption is indicated in *gray*. Reprinted with permission from Miyawaki et al., Curr. Opin. Chem. Biol. 7, 560 (2003).

mophore identical to GFP to generate its green intermediate [6]. Subsequently, the Cα-Nα bond of Gln^{66} oxidizes as the protein matures to become red (Fig. 2). The following section describes recent improvements in both YFP and DsRed maturation speed and/or fluorescence efficiency.

1.2 Improvements in Maturation of YFP

Two bright versions of YFP, Venus [7] and citrine [8], have recently been developed that mature quickly and efficiently, allowing for immediate detection of fluorescence signals after gene-introduction. Venus has a new mutation, F46L, and four common folding mutations, F64L, M153T, V163A, and S175G. The superiority of Venus to EYFP in terms of maturation is best observed following the re-naturation/re-oxidation profile of each protein. The chromophores of urea-denatured Venus and EYFP were reduced with 5 mmol/l dithionite [9], and re-naturation and re-oxidation were initiated by dilution at 37 °C (Fig. 3). Since oxidation is the rate-limiting step, the observed overall rate of fluorescence recovery under these circumstances should represent the rate of oxidation of the cyclized chromophore. The speed and yield of the re-naturation from denatured/reduced protein was significantly improved in Venus, which contains the F46L mutation (Fig. 3). To examine whether this mutation facilitates the maturation of any other *Aequorea* GFP variants, we introduced F46L into enhanced versions of blue, cyan, and green fluorescent proteins (Clontech). None of these mutants, however, displayed enhanced maturation

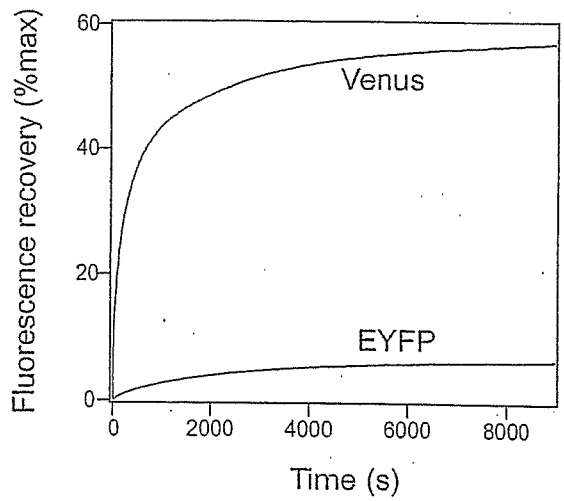

Fig. 3 Time course of fluorescence recovery of Venus and EYFP from their denatured/reduced state. For preparation of denatured/reduced protein samples, 5 mmol/l dithionite was added to denaturation buffer (8 mol/l urea and 1 mmol/l DTT). Recovery of fluorescence was initiated by a 100-fold dilution into re-naturation buffer (35 mmol/l KCl, 2 mmol/l $MgCl_2$, 50 mmol/l tris pH 7.5, 1 mmol/l DTT) at 37 °C. The emission at 530 nm was monitored by excitation at 515 nm. Reprinted with permission from Miyawaki et al., Curr. Opin. Chem. Biol. 7, 559 (2003). Copyright © 2003 Elsevier

[7]. On the other hand, the citrine version of YFP possesses a single mutation, Q69M [8].

Citrine and Venus have two main features in common. First, they both are yellow variants of GFP which have mutations, Q69M and F46L, respectively, which are specific to YFP. Second, they have similar backgrounds, arising from concerted efforts to improve the genetically encoded Ca^{2+} indicators, camgaroo [10] and pericam [11], respectively. As will be discussed below, camgaroo is a YFP variant into which calmodulin (CaM) has been inserted in place of Tyr145 of YFP; pericam was created by inserting a circularly-permuted YFP (cpYFP) between CaM and M13 (a CaM-target peptide). Since the original versions of camgaroo and pericam showed poor expression at 37 °C, their cDNAs were randomly mutated and screened in *E. coli* for maximal fluorescence. The Q69M and F46L mutations were found to be the most beneficial for improving the brightness of camgaroo and pericam, respectively, and these mutations were subsequently transferred into YFP to generate citrine and Venus. To engineer brighter GFP variants, therefore, it appears that the most efficient method may be to choose dimmer variants as parental constructs for mutagenesis. There is no guarantee, however, that the mutations discovered through this process will be effective for improving current bright variants. Though the crystal structures of citrine [8] and Venus [12] have been determined at 2.2 Å resolution, it is still unclear how the Q69M and F46L mutations act to accelerate the rate of oxidation of the Cα-Cβ bond of Tyr66.

The improved brightness should also be discussed in terms of the extent of quenching of the fluorophore by environmental factors. Among *Aequorea* GFP variants, YFPs are relatively acid sensitive, and uniquely quenched by halide ions, including chloride (Cl^-). Proton (H^+) and Cl^- synergistically affect the charge state of the chromophore of YFP, thereby suppressing its fluorescence. Citrine and Venus show increased resistance to both H^+ and Cl^- [7, 8].

1.3 Improvements in Maturation of DsRed

Compared with *Aequorea* GFP, DsRed has three unique features. First, the maturation process of DsRed includes a chromophore modification step which is responsible for changing its emission color from green to red (Fig. 2). Second, DsRed matures more efficiently at 37 °C than at room temperature, in contrast to *Aequorea* GFP, which folds preferentially at lower temperatures [13]. This may be directly traced to the differing water temperatures of the source organisms' habitats; *Aequorea victoria* is found in the Pacific Northwest, while *Discosoma* is native to the Indo-Pacific Ocean. Third, like many other Anthozoan GFP-like proteins, DsRed forms a tight tetrameric complex [14]. This tetrameric complex formation has been shown to be required for the development of red fluorescence [15], but it has not yet been determined which maturation step requires this process. Such tight oligomerization has probably evolved to maximize thermotolerance under conditions of intense tropical

sunlight. Very recently, Campbell et al. reported the successful engineering of monomeric RFP (mRFP1) from DsRed [16]. Their approach employed site-directed mutagenesis to break the tetrameric structure followed by random mutagenesis to rescue the original red fluorescence. The success of this work offers great hope regarding the conversion of other oligomeric fluorescent proteins into monomers. Another solution to the problem of RFP oligomerization reported by Campbell et al. [16] was to concatenate two dimer forming subunits of a mutant of DsRed with a spacer, which facilitates their dimer interactions through intramolecular contacts.

Incomplete chromophore modification of DsRed gives rise to residual green fluorescence, prohibiting the combined use of this molecule with green-emitting FPs in dual-color labeling experiments. The commercially available DsRed2 (Clontech) demonstrates only modest improvements in chromophore modification, but more recently, the release of engineered variants of DsRed known as T1 [17] and E57 [18] have enabled researchers to overcome the problems associated with slow and incomplete modification. Comparative analysis of these mutants in the context of the crystal structure of DsRed suggests available space around the chromophore is crucial for fast and complete modification [18]. Conversely, a long-lived green state can be advantageous for analysis of the history of gene expression in a cell. A new mutant of DsRed, E5, is particularly useful as it changes color from green to red in a predictable time course [19]. This feature makes it possible to use the ratio of green to red emission as an estimate of the time elapsed after initiation of reporter gene expression. Therefore, E5 functions as a fluorescent timer that yields temporal and spatial information regarding target promoter activity.

2
Engineering for Photoactivation and Photoconversion

2.1
Photoactivatable GFP

In the past two years, three new fluorescent protein variants have been generated that allow the selective activation or color conversion of fluorescent signal after specific illumination. The first variant, PA-GFP (photoactivatable GFP) [20] is based on wild-type *Aequorea* GFP, which has a bimodal absorption or excitation spectrum with two peak maxima, at 395 and 475 nm, corresponding to the protonated and the deprotonated states of the chromophore, respectively. When excited at 475 nm, wild-type *Aequorea* GFP emits maximal fluorescence at 503 nm, while excitation at 395 nm yields a maximum at 508 nm [2]. The latter large Stokes shift results from excited state deprotonation of the chromophore, as phenols become greatly more acidic in their excited states. Thus, excitation of the protonated chromophores gives emission at greater than 500 nm, similar to the direct excitation of the deprotonated chromophore.

Although the proton transfer is eventually reversible, the protonated chromophore is irreversibly isomerized to the deprotonated form upon intense illumination at 395 nm. The light transforms the species with the protonated chromophore, which absorbs at 395 nm, into the deprotonated species, which absorbs at 475 nm [2]. A recent cryospectroscopy, mass spectroscopy, and crystallography study on the photoconverted product showed that this photoconversion is a one-photon process paralleled by decarboxylation of a glutamic acid residue at position 222 [21]. Patterson and Lippincott-Schwartz found that substitution of histidine for threonine at position 203 was effective in decreasing the initial absorbance at 475 nm [20]. The resulting mutant, PA-GFP, exhibits up to a 100-fold increase in green fluorescence excitation at 488 nm when illuminated with 413-nm light.

2.2 Kaede

Around the same time, a green-emitting FP cloned from the stony coral *Trachyphyllia geoffroyi* was serendipitously discovered by Ando et al. to be useful as an optical cell marker [22]. The discovery occurred when the researchers accidentally left a test tube of the protein on a lab bench near a window, and found after a while that it had turned red. The naturally-engineered FP was named Kaede, the Japanese word for "maple leaf". Kaede contains a tripeptide, His^{62}-Tyr^{63}-Gly^{64}, which acts as a green chromophore that can be photoconverted to red. In its green state, it has two absorption peaks at 380 and 508 nm, corresponding to the neutral and ionized form, respectively. The neutral form of this molecule is highly sensitive to irradiation with UV or violet light (350–400 nm), which produce excitation and photoconversion. Interestingly, it has been observed that the photoconverted Kaede dissociates into 19- and 10-kDa fragments on SDS/PAGE. The structural basis for the green-to-red photoconversion has recently been presented [23]. As in *Aequorea* GFP, a chromophore, 4-(*p*-hydroxybenzylidene)-5-imidazolinone, derived from the

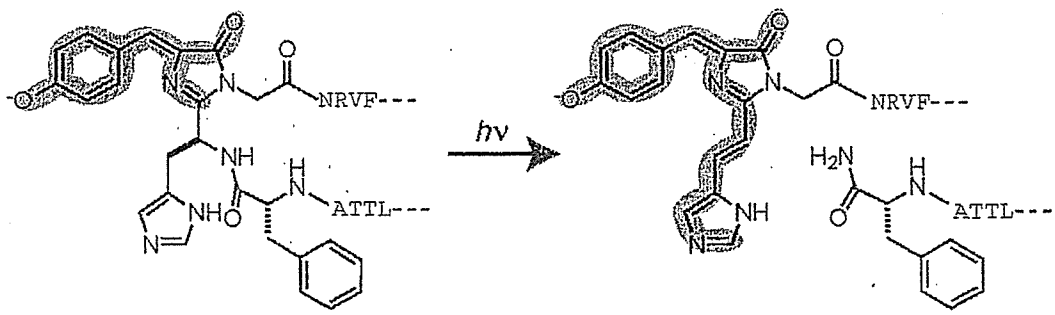

Fig. 4 Scheme for the formation and photo-induced extension of the chromophore of Kaede. Structures derived from Phe^{61}, His^{62}, Tyr^{63}, and Gly^{64} are drawn, and the neighboring amino acids (single-letter code) are added. π-conjugation for visible-light absorption is indicated in *gray*

tripeptide mediates green fluorescence in Kaede. UV irradiation causes an unconventional cleavage within Kaede protein between the amide nitrogen and the α carbon (Cα) at His^{62} via a formal β-elimination reaction, which requires the whole, intact protein for its catalysis. The subsequent formation of a double bond between His^{62}-Cα and -Cβ extends the π-conjugation to the imidazole ring of His^{62}, creating a new red-emitting chromophore, 2-[(1*E*)-2-(5-imidazolyl)ethenyl]-4-(*p*-hydroxybenzylidene)-5-imidazolinone (Fig. 4).

2.3 Kindling Fluorescent Protein

Lastly, Chudakov et al. showed that asCP, a unique GFP-like non-fluorescent chromoprotein from the sea anemome *Anemonia sulcata*, becomes fluorescent ("kindles") upon green light irradiation, with maximal emission at 595 nm [24]. Interestingly, asCP also has a histidine residue at position 203 (numbering in accordance with GFP alignment). More recently, they have generated a practically-useful mutant of asCP (designated KFP1) by replacing the alanine at position 148 with glycine [25]. KFP1 displays a roughly 30-fold increase in red fluorescence following excitation at 532 nm. This process is reversible, and can be controlled by both the light intensity level and the total light dose.

2.4 Histidine for Photochemical Reactions

It should be noted that all three of these variants carry histidine residues within or near the chromophore, suggesting the active involvement of histidine in photochemical reactions. Histidine, however, appears to play different roles depending on whether it is situated outside the chromophore at position 203 (PA-GFP and KFP1) or within the chromophore (Kaede). Studies by Ando et al. [22] and Chudakov et al. [24] have addressed the molecular mechanisms behind color variation occurring within individual coral animals. When exposed to sunlight, the tentacles and disk of the coral animals turn a shade of red in proportion to the degree of photoconversion. Then they revert to their previous colors as newly-synthesized proteins are added. Mechanisms such as this may be responsible for the great variety of color observed in coral reefs.

3 Engineering for Disruption of Oligomerization

Whether a fluorescent protein tends to form oligomers is an important consideration, as such interactions can interfere with the function of the host protein to which it is fused. Unfortunately, all of the *Anthozoan* GFP-like proteins

characterized so far form obligate oligomers [26]. While oligomerization does not prevent their use for reporting gene expression or marking cells, it does preclude their use in fusion protein applications. Similarly, fusion of DsRed, which normally forms a tetramer, to host proteins often disrupts their normal behavior, although there are some exceptions. As the monomeric RFP (mRFP1) matures ten times faster than its parental protein, it exhibits similar brightness to DsRed in living cells despite its lower molar extinction coefficient, fluorescence quantum yield and photostability. Because it is monomeric, mRFP1 has enabled red-fluorescence labelings that were not possible before with DsRed. Also, the excitation and emission maxima of mRFP1 are 584 and 607 nm, respectively, which gives good spectral separation from other FP signals. This work provides hope that other oligomeric FPs might also be converted into monomers. Indeed, the far-red variant HcRed1, made from a parent chromoprotein that seems to form obligate tetramers, has also been engineered to form dimers [27]. Similarly, a green-emitting FP recently cloned from *Galaxeidae* coral, Azami Green (AG) has been engineered to monomers (mAG) [28]. The anemone fluorescent protein epFP611 can function as a monomer, but only at low concentrations in the presence of detergent [29].

A further problem is the potential aggregation of fluorescent proteins, which impedes any cellular application and leads to cellular toxicity. Although the molecular mechanisms of FP aggregation remain unclear, there are two possible explanations. First, aggregation may be due to electrostatic or hydrophobic interactions between FPs. The possible contribution made by electrostatic interactions has been supported by recent work in which non-aggregating mutants were successfully generated by removing basic residues located near the amino termini of several fluorescent proteins [30], including DsRed. So, it may also be possible to make non-aggregating mutants by removing hydrophobic side chains on the surface of oligomeric complexes. It should be noted that *Renilla* GFP becomes soluble as a result of its dimerization; a hydrophobic patch becomes hidden at the dimerization interface and allows the surface of the dimer to become hydrophilic. The second possibility is that aggregation may follow FP oligomerization. Thus, the problem might be made worse still if host proteins are also oligomeric, as fusion to FPs might result in crosslinking into massive aggregates. Indeed, DsRed tends to produce more serious aggregation when fused to a host protein although, in an exception to this trend, fusion of DsRed to protein kinase C-γ retains the dynamic redistribution of the enzyme after stimulation. Overall, this aggregation problem would most easily be solved by using monomeric FPs.

Aequorea GFP has a propensity to weakly dimerize (Kd=0.1–0.3 mmol/l) [2]. Non-dimerizing CFP and YFP (mCFP and mYFP) have been constructed and utilized successfully in FRET experiments to determine how lipid-modified proteins assemble in the microdomains of the plasma membrane [31].

4
Engineering for Visualization of Cellular Functions

4.1
Genetically-Encodable Probes

In the past several years, various probes for cellular functions have been generated using FPs. Those probes employ simple GFP variants, circularly permuted GFP variants [10], or pairs of GFP variants that permit fluorescence resonance energy transfer (FRET) [32, 33]. Because the probes can be introduced by gene transfer techniques, they have significant advantages over conventional organic dyes. For instance, whereas conventional optical imaging of brain tissue stained with voltage-sensitive dyes is a noninvasive technique for recording the activities of a number of neurons simultaneously, it collects signals from all cell types including glial cells, which represent a large fraction of the total membrane surface in brain. By contrast, the selective introduction of genetically encoded probes into certain neurons has enabled the elimination of glial signals. Moreover, it is possible to place the probes within specific subcellular compartments where the desired signals predominate. The following section describes development of the probes that employ simple GFP variants or circularly permuted GFP variants.

4.2
Voltage Sensors

The prototype of the voltage-sensitive fluorescent protein is 'FlaSh' [34]. Insertion of wild-type GFP after the sixth transmembrane domain of a nonconducting mutant of the Shaker potassium channel has led to the generation of the sensor. In the construct, the voltage-driven rearrangement of the channel is converted into the change in fluorescence intensity of the GFP. It shows relatively complex and slow kinetics (τ_{off}>85 ms), suggesting that the structural rearrangement is related to the C-type inactivation of the channel. Recently, FlaSh has been significantly improved and diversified [35]. The substitution of various GFP variants has expanded its readout from single wavelength intensity modulating to dual wavelength ratiometric, and has produced probes with fast kinetics. In addition, mutations in the channel domain have tuned the probes. For example, the deletion of the N-terminal ball domain has improved the response rate and the Shaker S4 mutation L366A has negatively shifted the narrow dynamic range by approximately 30 mV, thereby enabling efficient detection of voltage changes around –60~70 mV occurring in retinal neurons.

Another genetically encoded voltage probe has been generated using a similar approach but a different channel. The probe termed 'SPARC' contains a mammalianized wild-type GFP inserted into an intracellular loop of a reversibly nonconducting form of the rat μI skeletal muscle voltage-gated sodium channel [36]. It can detect depolarizing pulses as short as 2 ms without inactivation

during extended depolarizations, which indicates that the fluorescence change is due to gating charge movement of a single domain of the channel.

4.3 Calcium Sensors

Our understanding of the structure-photochemistry relationships of GFP has enabled the development of genetic calcium probes based on a single GFP variant. Camgaroo-1 was constructed by inserting calmodulin (CaM) between positions 145 and 146 of YFP [10]. The Ca^{2+}-dependent conformational change of CaM induces the ionization of the chromophore, resulting in fluorescence increase of up to sevenfold. The chromophore development of this probe has been improved (camgaroo-2) by an amino acid substitution, Q69M [8].

Two groups fused circularly permuted green fluorescent proteins (cpGFPs) in which the amino and carboxyl portions had been interchanged around position 145 and reconnected by short spacers between the original termini, to CaM and its target peptide, M13. Chimeric proteins G-CaMP [37] and pericam [11] are fluorescent and their spectral properties change reversibly with Ca^{2+} concentration, probably due to the interaction between CaM and M13, leading to an alteration of the environment surrounding the chromophore.

G-CaMP is a single wavelength intensity modulating probe for Ca^{2+}. Fast mobilization of Ca^{2+} upon depolarization was observed in myotubes expressing the G-CaMP probe [37]. Recently, G-CaMP was applied to a functional analysis of odor-evoked patterns of activity in the neural assemblies in *Drosophila* antennal lobe [38]. The probe was expressed in olfactory receptor neurons or projection neurons, and patterns of glomerular activity were imaged in the antennal lobe presynaptically or postsynaptically, respectively. Odors elicited specific patterns of glomerular activity that were conserved in multiple flies, and the specific responsivity of a given glomerulus was found to be a consequence of the specificity of a single odorant receptor expressed by the incoming sensory neurons. Those observations are consistent with the "one neuron-one receptor" principle [39] that holds true for both vertebrate and insect olfactory systems.

Three types of pericam have been obtained by mutating several amino acids adjacent to the chromophore [11]. Of these, "flash pericam" becomes bright with Ca^{2+} like G-CaMP, whereas "inverse pericam" dims. On the other hand, "ratiometric pericam" has an excitation wavelength changing in a Ca^{2+}-dependent manner, thereby enabling dual excitation ratiometric Ca^{2+} imaging (Fig. 5A). Ratiometric pericam permits quantitative Ca^{2+} measurement by minimizing the effects of several artifacts that are unrelated to changes in free Ca^{2+} concentration ($[Ca^{2+}]$) (Fig. 5B). It has been successfully used to monitor changes in $[Ca^{2+}]$ in cardiomyocyte mitochondria. That study has demonstrated that mitochondrial $[Ca^{2+}]$ oscillates synchronously with cytosolic $[Ca^{2+}]$ during beating [40]. A laser-scanning confocal microscopy (LSCM) system has been modified for obtaining confocal images of Ca^{2+} using ratiometric pericam [41]. Rapid

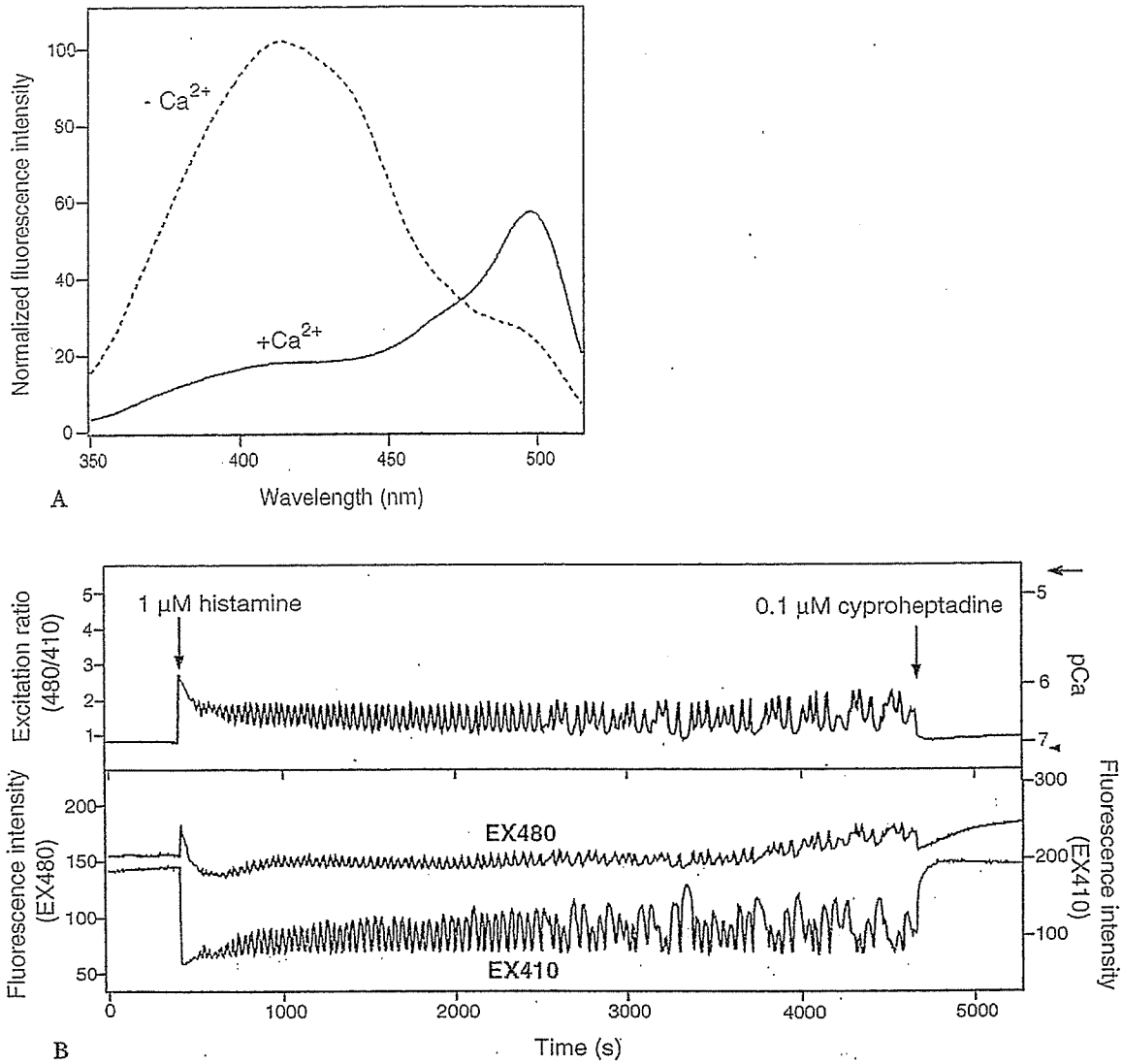

Fig. 5 A Excitation and emission spectra of ratiometric pericam in the presence and absence of calcium. B Typical $[Ca^{2+}]_i$ transients and oscillations induced by receptor-stimulations in HeLa cells expressing ratiometric-pericam. The sampling interval was 3~5 s. The right-hand ordinate calibrates $[Ca^{2+}]_i$ in µM with R_{max} and R_{min} indicated by an *arrow* and *arrowhead*, respectively. Reprinted with permission from Nagai et al., Proc. Natl. Acad. Sci. USA 98, 3197 (2001). Copyright © 2001 National Academy Sciences, USA

exchange between two laser beams has been achieved using acousto-optic tunable filters. Samples are scanned on each line sequentially by a violet laser diode (408 nm) and a diode-pumped solid state laser (488 nm). In this way, the ratios of the excitation peaks can be obtained at frequencies of up to 200 Hz, which enables visualization of Ca^{2+} dynamics within a motile mitochondrion.